Structural Inversion of Micellar Block Copolymer Thin Films

Yuan Li,[†] Luciana Meli,[‡,§] Kwon T. Lim,[||] Keith P. Johnston,*[,†,‡] and Peter F. Green*[,§]

Graduate Program in Materials Science and Engineering, Department of Chemical Engineering, The University of Texas at Austin, Austin, Texas 78712, Department of Materials Science and Engineering, The University of Michigan, Ann Arbor, Michigan 48109, and Division of Image and Information Engineering, Pukyong National University, Pusan 608−739, South Korea

Received April 30, 2006; Revised Manuscript Received July 6, 2006

ABSTRACT: Polystyrene-*b*-poly(1,1′,2,2′-tetrahydroperflurooctyl methacrylate) (PS-*b*-PFOMA) thin films, cast from a cosolvent mixture of Freon 113 and toluene onto Si/SiO_x substrates, form spherical micelles; the cores are composed of PFOMA chains with a PS corona. Upon exposing the films to supercritical CO_2 (Sc-CO_2), the morphology inverts, wherein the core is composed of PS chains and the PFOMA chains constitute the corona. In each case, the free surface and polymer/substrate layers are enriched with PFOMA. The size of the PS cores is found to increase with decreasing Sc-CO_2 activity. This size variation is discussed in light of recent theoretical developments that account for the effect of Sc-CO_2 activity on PS−CO_2 interfacial tension and chain stretching of the corona versus the core.

1. Introduction

Block copolymers are exploited for a diverse range of applications, which include templates to create periodic patterns for nanolithography and for "bottom up" fabrication in microelectronics.[1−11] Important challenges are typically associated with processing to control the long-range orientation and lateral ordering of the nanometer-scale domains. Strategies that use external fields are employed such as electric fields,[6,12] graphoepitaxy,[11,13] chemical patterned substrates,[14−17] for thin films, and shear[18,19] and temperature gradients,[20] for bulk.

Liquid and supercritical CO_2 have been shown to be attractive alternatives to organic solvents in many polymer processes.[21−24] Sorption of CO_2 into polymers can cause significant swelling and plasticization, lowering the glass transition temperature T_g of amorphous polymers, inducing crystallization in crystalline polymers,[22,25−28] and influencing order−disorder transition (ODT) temperatures and ordering kinetics of block copolymers.[29−32] Aside from the environmentally benign properties and easily accessible critical conditions (T_c = 31 °C and P_c = 73.8 bar) of CO_2, the solvent strength of CO_2 can be tuned markedly with pressure and temperature. While most research has focused on bulk polymer systems in Sc-CO_2,[22] the effects of Sc-CO_2 on thin polymer films have received far less attention. Studies in our laboratories have suggested a strong influence of Sc-CO_2 on the sorption, on the glass transition temperatures (T_g), on the morphological instability of homopolymer thin films, and on the ordering transition of block copolymer thin films.[29,33−37]

In this study, we show that polystyrene-*b*-poly(1,1′,2,2′-tetrahydroperflurooctyl methacrylate) (PS-*b*-PFOMA) thin films spin-cast, using a cosolvent of Freon 113 and toluene, onto Si/SiO_x substrates, form micelles with a PFOMA core and PS corona. We show that, upon annealing in a compressed solvent, supercritical carbon dioxide (Sc-CO_2), the structure is inverted and the PS chains, which formally constituted the continuous phase (corona), now formed the core phase and the PFOMA chains formed the continuous phase. The sizes of PS cores increased with increasing Sc-CO_2 annealing temperatures at a constant pressure. These observations are rationalized based on the change of interfacial tension between PS and CO_2 as well as the relative stretching of PS and PFOMA chains as Sc-CO_2 activity varies.

* Corresponding authors. E-mail: pfgreen@umich.edu (P.F.G.).
[†] Graduate Program in Materials Science and Engineering, The University of Texas at Austin.
[‡] Department of Chemical Engineering, The University of Texas at Austin.
[§] Department of Materials Science and Engineering, The University of Michigan.
[||] Division of Image and Information Engineering, Pukyong National University.

2. Experimental Section

In this section, the synthetic procedures used to prepare the polymers and the processing strategies, involving Sc-CO_2 annealing, used to prepare the films, are described. In addition, the characterization techniques, scanning transmission electron microscopy (STEM) and scanning force microscopy (SFM), used for morphological analysis, X-ray photoelectron spectroscopy (XPS) for surface compositional analysis, and spectroscopic ellipsometry for analyzing the swelling of the films in Sc-CO_2, are described.

2.1 Synthesis of Materials. *2.1.1. Preparation of PSt-Br Macroinitiator by ATRP.* A Florence (round-bottom) flask containing a Teflon coated magnetic stir bar was charged with CuBr and bipy(2,2′-dipyridyl) (Bpy). Prior to use, the flask was vacuumed and back-filled with dry nitrogen several times. Ethyl-2-bromoisobutyrate (EtBr) and styrene (St) were then added under nitrogen atmosphere with the ratio of [St]/[EtBr]/[CuBr]/[Bpy]as 19.2:1:1:3. The flask was subsequently placed in an oil bath and heated to 110 °C with continuous stirring for 24 h. After polymerization, the reaction mixture was diluted with tetrahydrofuran (THF) and passed through a neutral Al_2O_3 column to remove the catalyst. The solution was then precipitated into methanol, and the polystyrene (PSt-Br) product was filtered and dried in a vacuum. The molecular weight of polystyrene (PSt-Br) was determined to be 27 000 g/mol by ^{1}H NMR, with the polydispersity of 1.12 determined by gel permeation chromatography (GPC).

2.1.2. Preparation of PSt-b-PFOMA Block Copolymer by ATRP. PSt-Br macroinitiator, CuCl, and Bpy were placed in a Florence flask with Teflon coated magnetic stir bar. After the flask was vacuumed and back-filled with dry nitrogen several times, trifluorotoluene (TFT) was added into the flask. The solution was degassed with dry nitrogen, and then 1,1′,2,2′-tetrahydroperfluorooctyl methyl methacrylate (FOMA) was introduced to the solution

10.1021/ma060960r CCC: $33.50
Published on Web 09/09/2006

Table 1. Characteristic Properties of PS and PFOMA in the Diblock

parameters	PS	PFOMA
M_n (kg/mole)	27	127
T_g (°C)	100	50[38]
ρ (g/cm^3)	1.06	1.53[a]
M_o (g/mole)	104	432
N	260	294
γ (dyn/cm)	41	<11[40]
volume fraction: f	0.25[b]	0.75[b]
volume per monomer: V (nm^3)	0.167[39]	0.389[c]
end-to-end distance in unperturbed state: l_e (nm)	10.5[39]	14.5[c]
maximum stretching length: l_m (nm)	80.1[d]	90.5[d]

[a] Data provided by Dr. Gabriel Luna-Barcenas, to be published. [b] $f = (M_{PS}/\rho_{PS})/(M_{PS}/\rho_{PS} + M_{PFOMA}/\rho_{PFOMA})$. [c] Based on: $V_{PFOMA}/V_{PS} = (l_{ePFOMA}/l_{ePS})^3 = (M_{oPFOMA}/\rho_{PFOMA})/(M_{oPS}/\rho_{PS})$. [d] $l_m = 2N \times 1.54A$.

with the ratio of [FOMA]/[PSt-Br]/[CuCl]/[Bpy] as 198:1:1:3. Polymerization was performed at 110 °C in a nitrogen blanket for 37 h. After polymerization, the mixture was diluted with TFT and passed through the Al_2O_3 column. Then the reaction solution was precipitated into heptane, and the resulting product was filtered and dried in a vacuum for 12 h. After extraction with cyclohexane to remove unreacted macroinitiator, the polymer was filtered and dried in a vacuum. The molecular weight of the resulting polystyrene-*b*-poly(1,1′,2,2′-tetrahydroperflurooctyl methacrylate) (PS-*b*-PFOMA) block polymer was determined to be 154 000 g/mol by comparing the signal of PSt and PFOMA block in ^{1}H NMR spectrum.

2.2. Thin Film Preparation and Characterization. The block copolymer of PS-*b*-PFOMA (properties listed in Table 1[38−40]) was dissolved using a cosolvent of 1,1,2-trichlorotrifluroethane (Freon 113) and toluene. The resulting transparent solutions have a weight concentration of 0.5−1% polymer and 15−25% toluene. Dynamic light scattering (DLS) measurements were performed using a Brookhaven laser light scattering instrument (Brookhaven Instruments Corp.), with a diode laser (24 mV) at a wavelength of 659 nm at 20 °C.

Thin films were prepared by spin-casting the solutions onto silicon wafers with a native oxide layer (Wafer World Inc.), and the thicknesses of the films were measured by spectroscopic ellipsometry (J. A. Wollam Co., Inc.). Different thicknesses were obtained by controlling the spin rate and concentration of the copolymer solutions. Samples for STEM imaging were prepared by floating as-cast films into water and picking up with electron transparent silicon nitride windows (SPI supplies) to achieve film uniformity.

2.3. Supercritical CO_2 Annealing. The samples (supported by either Si/SiO_x or silicon nitride windows) were loaded into a fixed volume cell, which was subsequently sealed and pressurized with carbon dioxide (Air Products, >99.999%) using a manual pressure generator (High-Pressure Equipment Co.). The pressure was controlled with a strain gauge pressure transducer (Sensotec) calibrated to within $\pm 7 \times 10^{-3}$ MPa. Typically, the temperature was controlled to ±0.1 °C by immersing the pressure cell into a water bath equipped with a temperature controller (Julabo, Inc.). For high-temperature (above 100 °C) experiments, the pressure cell was wrapped by heating tapes that were connected to a temperature controller (Omega Engineering, Inc). The diblock was in a rubbery state in all conditions studied (35, 50, 75, 140 °C and at the Sc-CO_2 pressure of 13.8 MPa). After a certain annealing period (varying from 10 h to 10 days), the cell was cooled to approximately 25 °C and depressurized by venting Sc-CO_2 as a vapor from the top of the cell. In the process of depressurization and cooling, the films returned to glassy state and the morphology of the films was frozen.

2.4. Morphological Analysis Using Scanning Force Microscopy (SFM) and Scanning Transmission Electron Microscopy (STEM). Morphological characterization of the films was achieved by a combination of scanning force microscopy (SFM) and scanning transmission electron microscopy (STEM). SFM measurements were performed in tapping mode using a Nanoscope IV/Dimension 3100 (Digital Instruments). Identical morphology was observed by SFM for samples supported by Si/SiO_x or silicon nitride windows. Figure 1 is indicative of the micellar structure of the films formed from the cosolvent; the images are discussed in further detail in the next section.

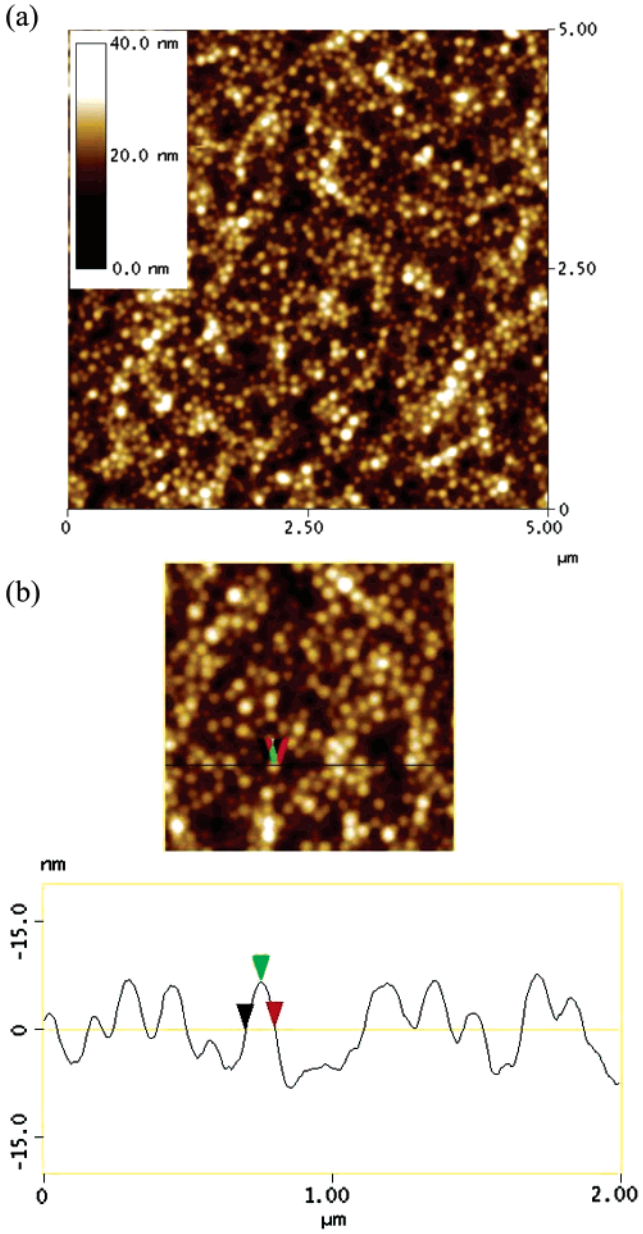

Figure 1. SFM topography (a) and the corresponding line scan (b) of a PS-*b*-PFOMA film ($h = 90$ nm) after spin-casting from solution onto Si/SiO_x substrate. The scan sizes are 5 μm in (a) and 2 μm in (b). The colored triangles in the topography (b) are corresponding to those in the line scan. This particular circular feature has a diameter of 101.56 nm (between leftmost and rightmost triangles) and a height of 7.3 nm (between leftmost and middle triangles).

Considerably more detail of the morphological structure of the film can be obtained using STEM. STEM imaging was performed using a JEOL 2010F transmission electron microscope operating at an accelerating voltage 200 kV in scanning mode, using a high-angle annular dark field (HAADF) detector. HAADF imaging, also called *Z*-contrast imaging, enabled observation of the species present based on differences in atomic numbers (*Z*), densities, and sample thicknesses. Thus, for copolymer samples without vapor staining, contrast was provided by the difference between the densities of the two constituent blocks; the denser PFOMA regions appear brighter than the PS domains. In some cases, samples were exposed

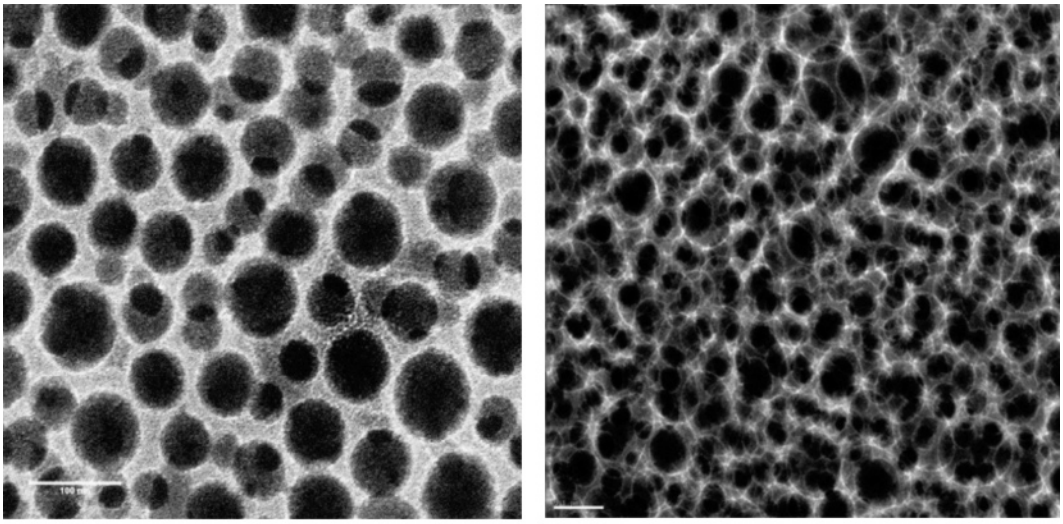

(a) (b)

Figure 2. HAADF−STEM images of RuO_4 stained PS-*b*-PFOMA films after spin-casting: (a) a 72 nm film presenting two layers of micellar aggregates; (b) an even thicker film with more layers of micellar aggregates. The scale bars in both images are 100 nm.

to the vapor of an aqueous RuO_4 solution (SPI supplies) for 5 min to selectively stain the PS-rich domains. In this case, the selectively adsorbed ruthenium compound provides brighter contrast to the PS phase. Figure 2 shows a typical image of an as-cast film with the circular PFOMA cores and the PS corona (continuous phase). This will be discussed in further detail later.

2.5. X-ray Photoelectron Spectroscopy (XPS). XPS measurements were performed on PS-*b*-PFOMA films with thicknesses on the order of 100 nm using a Physical Electronics (PHI) model 5700 spectrometer employing a monochromatic Al $K\alpha_{1,2}$ source. XPS spectra of PS (30 kg/mole, from Pressure Chemical) and poly(1,1′-dihydroperflurooctyl methacrylate) (PDHFOMA) (M_n = 100 kg/mole, synthesis procedure was described elsewhere[41]) homopolymer films were taken as references. The binding energy of the instrument was calibrated by using $Au_{4f7/2}$, $Cu_{1p3/2}$, and $Ag_{3d5/2}$. Typical operating conditions were the following: 1×10^{-9} Torr chamber pressure; 14 kV; 250 W for the Al X-ray source. Survey scans from 0 to 1000 eV were taken with the pass energy of 93.9 eV. High-resolution elemental scans of the C_{1s}, F_{1s} regions were collected with the pass energy of 11.75 eV at takeoff angles of 45 and 75° between the sample and analyzer, where the sampling depth was estimated to be 5.7 and 7.8 nm, respectively.[40] The atomic percentages of C and F were determined using XPS peak areas and the appropriate instrumental sensitivity factors. To ensure that the samples were not damaged by long-time X-ray exposure, three high-resolution elemental scans were carried out subsequently, where the resulting C and F atomic percentages were in good agreement within experimental error ranges. In some experiments, the topmost part of the samples were etched by Argon (Ar^+) ion sputtering at 2 kV voltage and 1 μA beam current (2 mm × 2 mm area) for 5 s, and high-resolution elemental scans of C_{1s} and F_{1s} regions were then carried out.

2.6. In Situ Swelling Experiments. Spectroscopic ellipsometry (J. A. Wollam Co., Inc.) was used to measure in situ swelling of PS (M_n = 30 kg/mole), PDHFOMA (M_n = 100 kg/mole) homopolymers, and PS-*b*-PFOMA copolymer films (thicknesses between 100 and 120 nm) in Sc-CO_2. Detailed experimental setup and analysis procedures had been described elsewhere.[37] The swelling percentage was determined by the following equation assuming uniaxial swelling

$$\mathrm{Sw\%} = \frac{\Delta V}{V_0}(\%) = \frac{h - h_0}{h_0} \times 100\% \qquad (1)$$

Here V_0 is the initial volume of the film, h is the thickness of the swollen film, and h_0 is the initial thickness of the polymer films determined by spectroscopic ellipsometry at 0 psig.

Table 2. Atomic Ratio between Fluorine and Carbon from XPS Data for As-Cast Films

samples	angle (deg)	sputter time (s)	*C* (%)	*F* (%)	*F*/*C* (expt)	*F*/*C* (calcd)
PS	45	0	99.95	0.05	0	0
PDHFOMA[a]	45	0	43.29	56.71	1.31	1.25
PTHFOMA[b]						1.08
PS-*b*-PFOMA	45	0	55.31	44.69	0.81	0.68
PS-*b*-PFOMA	75	0	59.40	40.60	0.68	0.68
PS-*b*-PFOMA	75	5	77.93	22.07	0.28	0.68

[a] PDHFOMA: Poly(1,1′-dihydroperflurooctyl methacrylate). [b] PTHFOMA: Poly(1,1′,2,2′-tetrahydroperflurooctyl methacrylate).

3. Results and Discussion

This section is divided into three parts. The morphology of the as-cast films, which form a micellar structure (PFOMA core and PS corona), is first discussed. In the section that follows, the evolution of the structure during Sc-CO_2 annealing is discussed; it is shown that the structure inverts, wherein the PS segments constitute the cores of the micelles and PFOMA segments form the corona. Finally, experiments and theory describing the variation of the size of the micelles with Sc-CO_2 activity are discussed.

3.1. Self-Assembly of PS-*b*-PFOMA Diblock into Micelle-like Aggregates in Thin Films after Spin-Casting. Typical SFM image of the topography of a PS-*b*-PFOMA thin film supported by the Si/SiO_x substrate is shown in Figure 1a. Figure 1b shows a small region of the image in Figure 1a and an accompanying line scan. The observed circular regions possess an average feature height of 6.7 ± 1.5 nm and an average diameter of 105 ± 18 nm. Figure 2a shows an STEM image of a stained 72 nm thick as-cast sample. It is evident from this figure that the micelles are composed of PFOMA cores embedded in a continuous PS (corona) matrix; the overlapping circular features reveal the presence of two layers of micellar aggregates across the film thickness. The existence of multiple layers of micelles is evident from Figure 2b, the image of a much thicker film.

Having described the internal structure of the as-cast films, the free surface structure is now described. Table 2 shows the XPS results for as-cast PDHFOMA and PS-*b*-PFOMA films; three observations can be made. First, as the takeoff angle increases from 45 to 75°, the experimental *F*/*C* ratio for PS-

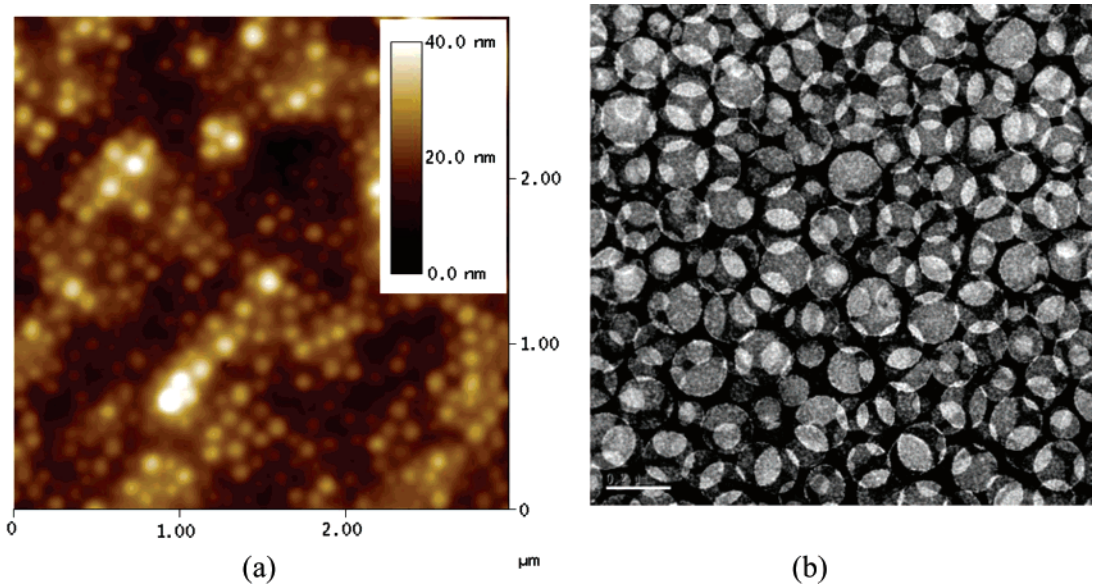

Figure 3. (a) SFM topography of a PS-*b*-PFOMA film ($h = 88$ nm) after annealing at Sc-CO_2, 75 °C, 13.8 MPa for 3 days. (b) HAADF−STEM image of a RuO_4 stained PS-*b*-PFOMA thin film sample supported on SiN grid after annealing at Sc-CO_2, 75 °C, 13.8 MPa for 3 days. The scale bar represents 200 nm.

b-PFOMA thin films decreases from 0.81 to 0.68. This decrease indicates that, as expected, PFOMA chains are more segregated to the free surface than PS chains due to their lower surface energy (<11 dyn/cm). Second, the *F*/*C* ratios for both takeoff angles are either comparable or slightly larger than the theoretical value for PS-*b*-PFOMA. They are, however, smaller than the theoretical values for PFOMA. One would anticipate that the surface of PS-*b*-PFOMA films is composed entirely of PFOMA because the surface tension of PFOMA is substantially lower than that of PS. However, our XPS data suggests that the top 8 nm of copolymer films consist predominantly, but not entirely, of PFOMA. This is not surprising in light of the nonequilibrium nature of the spinning process. Third, the last XPS experiment shows that the *F*/*C* ratio drops dramatically after sputter etching of the topmost layer of the film. This large decrease also suggests that surface PFOMA segregated layer is very thin and that there is a PS-rich domain below this topmost thin layer. Our results are consistent with the work by Arnord et al.,[40] where they observed the surface of PDMAEMA-*b*-PFOMA films consisted primarily of PFOMA and that as the XPS takeoff angle increased, the surface concentration of PFOMA decreased rapidly. Because PFOMA chains form the core of the aggregates, the surface segregated PFOMA layer can be either a half-lamella-like structure[42,43] or a thin layer with the fluorinated side chains aligned toward the surface. However, the thickness of this layer (less than 8 nm) is too small for a half-lamella layer (see Table 1). Therefore, we conclude that a few nanometer thin PFOMA layer, with the fluorinated side groups facing outward, resides at the free surface.

The micellar formation process is now discussed. Amphiphilic block copolymers are known to self-organize into aggregates in water or in selective organic solvents. The adsorption or covalent attachment of block copolymer micelles to solid surfaces has attracted appreciable attention, experimentally, during the past decade.[44−53] Theoretical work has been rare, and the effects of interfaces and confinement on the structure of spherical micelles are not well understood. Work by Liquore shows that, unlike micelles in solution, the structures of surface micelles can be strongly affected by an absorbing solid surface, and that the critical surface micelle concentration (CSMC) can be different from the value for bulk micelles.[50] It is found that, if the contact angle between the core block and the surface is less than a universal value of $\theta_o^C \sim 51°$, then surface micelles appear at a CSMC much lower than the critical micelle concentration (CMC) in bulk solution.[50]

It is evident that micelles do not exist in solution; instead, they form during the spin-casting process. Our DLS measurements of the PS-*b*-PFOMA solutions showed no evidence of particles within a reasonable size range. Furthermore, solubility tests were performed to examine the solubility of PS and PDHFOMA in the cosolvent mixture. Specifically, a saturated solution of PS in the cosolvent was prepared so that adding one drop of Freon 113 would make the solution turbid and another drop of toluene would make the solution clear. We found that the solubility of PS and PDHFOMA in the cosolvent is definitely higher than the concentration of the solutions used to spin-cast films, suggesting that the surface aggregates were formed upon spin-casting. In addition, because the majority of the solvent used was Freon 113, a good solvent for PFOMA, it is expected that any possible aggregates in the solution would possess a PFOMA shell, in contrast to the STEM observations. Therefore, we believe that the surface PS-*b*-PFOMA aggregates were formed upon spin-casting due to the fast evaporation of Freon 113.

The block copolymers form micelles only during the spin-coating process; similar results has been observed in other systems.[54,55] Lin et al. found that polystyrene-*b*-poly(ethylene oxide) (PS-*b*-PEO) formed ordered arrays of cylindrical domains perpendicular to the substrate after spin-casting from a benzene solution.[55] This ordering of PS-*b*-PEO after spin-casting can be attributed to two factors. First, benzene is good solvent for both blocks, hence the diblock was phase mixed in the solution. Second, the interfacial tension between PS and PEO blocks increases abruptly as benzene evaporates during the spin-casting process, leading to the formation of phase-separated domains. For the PS-*b*-PFOMA system, upon spin-casting, Freon 113, which possesses a larger vapor pressure (285 mmHg at 20 °C), evaporates at much faster rates than toluene, with a vapor pressure of 22 mmHg at 20 °C. Hence, with the evaporation of Freon 113, the quality of the solvent becomes progressively poorer for the PFOMA block and the effective concentration

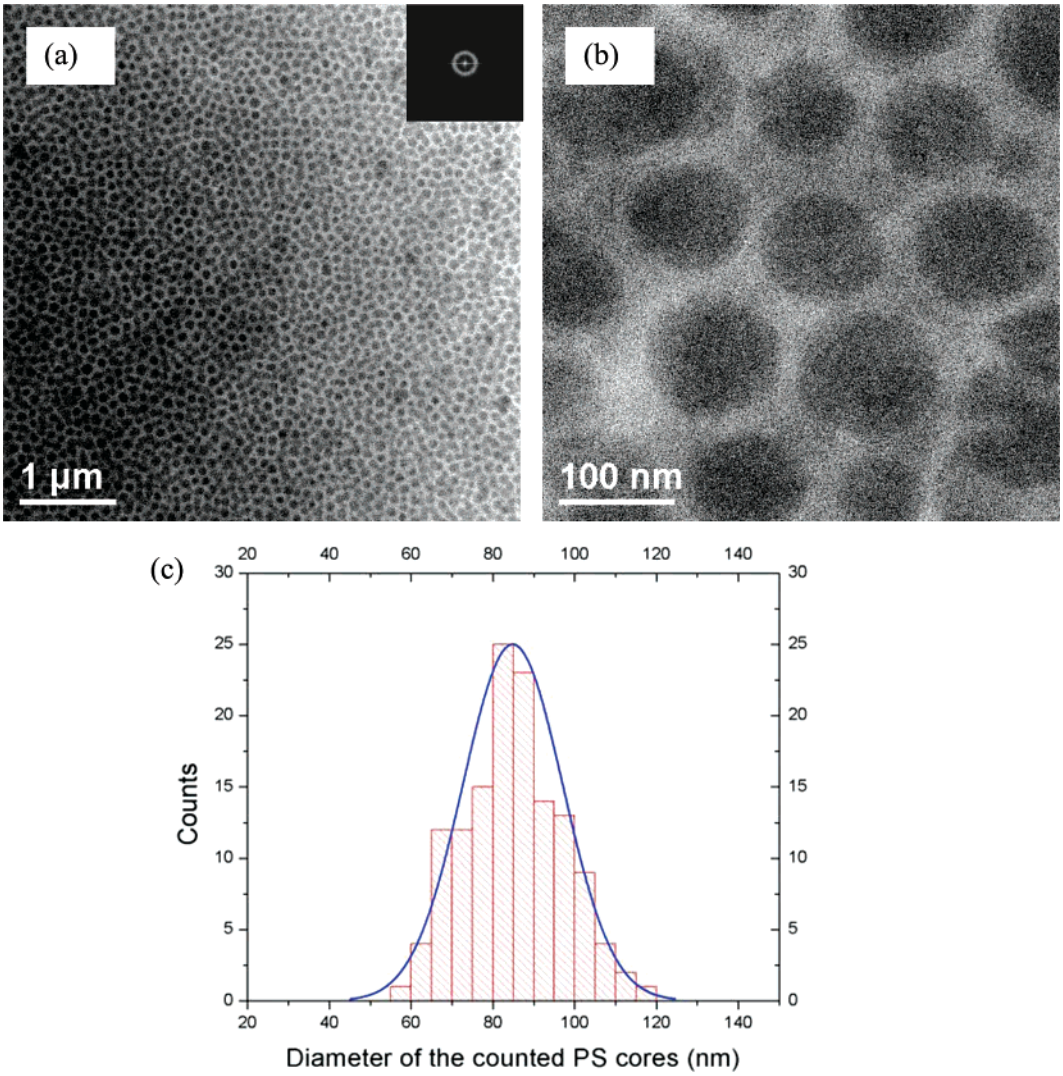

Figure 4. (a, b) HAADF−STEM images of a PS-*b*-PFOMA thin film sample supported on SiN grid after annealing at Sc-CO_2, 75 °C, 13.8 MPa for 3 days. (c) The size distribution of PS cores in (a).

of the copolymer increases above the critical micelle concentration (CMC), leading to micellar formation.

In summary, the combination of SFM and STEM images indicates that PS-*b*-PFOMA films self-organize into spherical micelle-like aggregates with PFOMA composing the core after spin-casting. The XPS data revealed the existence of PS-rich domains below a thin PFOMA-rich surface layer, with thickness much less than one-half the domain spacing.

3.2. Effects of Supercritical CO_2 Annealing on the Morphologies of PS-*b*-PFOMA Thin Films. *3.2.1. Inversion of the Core−Shell Composition of PS-b-PFOMA Aggregates in Sc-CO_2.* Upon Sc-CO_2 annealing of the as-cast film, the structure underwent an inversion; the PS chains now constituted the cores. Figure 3 shows both the SFM and STEM images of PS-*b*-PFOMA samples annealed in Sc-CO_2 at 75 °C, 13.8 MPa. The SFM image (Figure 3a) of the Sc-CO_2 annealed film shows topography of random arrays of circular features, very similar to those before Sc-CO_2 annealing. However, the RuO_4 stained *Z*-contrast image (Figure 3b) reveals that the darker PFOMA domain forms the matrix (corona) of the film, whereas the brighter stained PS chains form the cores of the spheres in this multilayered structure. This reversal in core−shell composition is not surprising due to the fact that Sc-CO_2 is a selective solvent for fluoropolymers.[56]

The structure of the film was confirmed by STEM images of unstained films (without RuO_4 staining, the contrast between PS and PFOMA is only strong enough to show one layer of micellar aggregates), as shown in Figure 4a and b. The denser (higher *Z*) PFOMA regions (1.53 g/mL) of the film should appear brighter than the PS regions (1.06 g/mL). Figure 4a clearly shows black circular features in a bright, hazy matrix, further confirming that PS constitutes the cores after Sc-CO_2 annealing. It is evident that CO_2 annealing is also responsible for an increased degree of lateral ordering, as shown by the ring that appears in the FFT of the image (the inset in Figure 4a). Detailed size measurements (size distribution shown in Figure 4c) of Figure 4a gave an average diameter of PS core and center-to-center distance between two cores as $D = 85 \pm 12$ nm, and $L = 115 \pm 15$ nm, respectively, and the nearest-neighbor distance obtained from Fourier transform (FT) was $l = 110$ nm.

Table 3 compares the XPS results of Sc-CO_2 annealed PS-*b*-PFOMA films with those after spin-casting. It is clear that the *F*/*C* ratios at both takeoff angles increase upon Sc-CO_2 annealing, suggesting that the surface of the Sc-CO_2 annealed films is pure PFOMA. In addition, the *F*/*C* ratios for Sc-CO_2 annealed films were even larger than the calculated *F*/*C* ratio for PFOMA homopolymer, indicating that the perfluorocarbon

Table 3. Atomic Ratio between Fluorine and Carbon from XPS Data for PS-*b*-PFOMA Films after Sc-CO_2 Annealing at 75 °C and 13.8 MPa

	F/*C* ratio			
XPS takeoff angle (deg)	after spin-casting	after CO_2 annealing	calcd for the diblock	calcd for PFOMA
45	0.81	1.13	0.68	1.08
75	0.68	1.31		

side chains are more biased toward the free surface due to the strong affinity between PFOMA and CO_2.

We conclude this section by first pointing out that, in addition to the free surface, a layer of PFOMA resides at the PS-*b*-PFOMA/SiO_xSi interface due to the carbonyl groups. This is the same reason the PMMA component of a PS-*b*-PMMA diblock preferentially wets SiO_x/Si.[29,57,58] Second, the strong affinity between PFOMA and the Sc-CO_2 leads to a reversal of the internal core−shell composition of the micelles. The schematics in parts a and b of Figure 5 summarize the structures of the as-cast and the Sc-CO_2 annealed films, respectively.

3.2.2. Shape of the PS-b-PFOMA Micellar Aggregates. The micellar size and shape are now discussed. Following the work by Eisenberg and co-workers,[39] the size of a typical block copolymer micelle can be estimated from the degree of stretching, S_c, of the core block and is specified by

$$S_c = \frac{D}{2l_e} \tag{2}$$

Here, D is the diameter of the micelle cores. For the micelles with PS cores in Figure 5b, l_e denotes the end-to-end distance of PS block in an unperturbed state and is listed in Table 1. For most block copolymer micelles, S_c is found in the range of 0.7−1.5.[39] Thus, a maximum value of D of $2 \times 1.5 \times 11 = 33$ nm is expected for PS cores. However, the experimentally determined values of the PS core diameter in Figure 4a is 85 nm, more than twice the calculated value. This discrepancy can be explained by the deformation of spherical micelles confined on a solid substrate.[59] This increase in size can be understood by the fact that the carbonyl groups of the PFOMA chains at the substrate have a strong affinity to the polar Si/SiO_x.[29,57,58] Consequently, the micellar cores develop an ellipsoid-like shape, wherein the height of the ellipsoid is smaller than its radius on the plane parallel to the substrate (the core radius measured from the *Z*-contrast images is the major axis of the ellipsoid-like aggregates, which is highly extended due to this confinement effect). The minor axis, only observable from cross-section imaging (not performed in this study), should be approximately equal to l_e. It is noteworthy that this deformation of the spherical micelle cores is analogous to the phenomena that the volume pervaded by a polymer chain changes from a spherical to ellipsoidal shape when confined in ultrathin films.[60]

Before concluding this section, the effect of rapid CO_2 desorption on the aggregate size is discussed. Ex situ ellipsometry measurements of PS-*b*-PFOMA films showed a thickness increase of about 12−18% after annealing at 75 °C in Sc-CO_2. Although this degree of swelling is measurable, it is much lower than the swelling ratio of 47% determined by in situ ellipsometry on PS-*b*-PFOMA films under the same condition. We expect that, upon desorption of CO_2, the diblock films rapidly cross the glass transition and become "frozen". The "frozen" PS core would, therefore, have a size somewhere between the pure unswollen PS and the CO_2 swollen PS. For PS, in situ ellipsometry experiments at 75 °C and 13.8 MPa give a swelling ratio of about ~9.3%, which corresponds to an increase of 3%

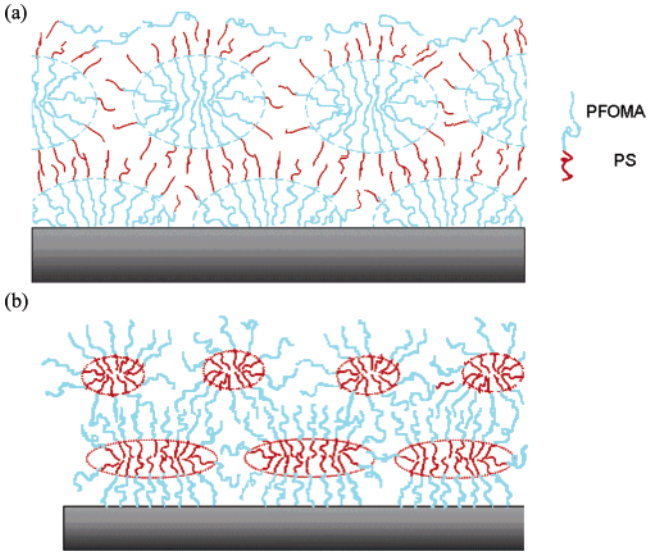

Figure 5. Schematic representations of the PS-*b*-PFOMA surface aggregates after spin-casting from the solution onto Si/SiO_x substrate (a) and annealing under Sc-CO_2 (b). Light-blue chains are PFOMA; red chains are PS. Note in (a) an ultrathin layer of PFOMA segregated layer (with the fluorinated side groups aligned toward the outer face) is drawn on free surface. On the substrate interface, a layer of highly deformed PFOMA cored hemimicelles is drawn due to the strong interaction between the carbonyl group and SiO_2.

in the diameter of PS core. Thus, the effect of CO_2 swelling on the measured PS core sizes after CO_2 desorption is negligible and within experimental errors. On the other hand, PFOMA swells substantially more in CO_2, and the length of the corona is highly underestimated from the ex situ STEM measurements.

3.3. Effects of Supercritical CO_2 Annealing Temperature on the Core Sizes of PS-*b*-PFOMA Aggregates. In this section, the effects of Sc-CO_2 annealing temperature on the morphologies of the copolymer films are examined, experimentally and theoretically. Parts a−d of Figure 6 show STEM images of unstained PS-*b*-PFOMA films annealed under Sc-CO_2 at four temperatures while the pressure was fixed at 13.8 MPa. It is clear that, as the Sc-CO_2 annealing temperature increased from 35 to 140 °C, the sizes of the PS cores increased continuously, as seen in the increase of D, L, and l (Figure 6e).

To further understand the effect of Sc-CO_2 temperature on relative swelling of the two blocks, the swelling isotherm for PS, PDHFOMA homopolymer thin films in Sc-CO_2 at 35 and 50 °C was measured by in situ ellipsometry (Figure 7a). At a constant pressure, as temperature increases from 35 to 50 °C, the swelling for PDHFOMA decreases appreciably. On the other hand, the change in swelling of PS films with temperature is very small. It is noteworthy that both curves at 35 °C show anomalous swelling peaks in the regions where the compressibility of Sc-CO_2 is at maximum. These unique anomalous swelling maximum of polymer thin films in Sc-CO_2 was discovered by Sirard et al.[36] and will be examined into further detail in a subsequent paper.

The swelling isotherms can be plotted against Sc-CO_2 activity to combine the effect of both temperature and pressure (Figure 7b). As has been discussed in our previous work, the swelling of a rubbery polymer in Sc-CO_2 is only dependent on CO_2 activity.[36] Because the T_g of PFOMA is only 50 °C at ambient conditions and is even more depressed under Sc-CO_2, the difference between the two isotherms of PDHFOMA films is, within experimental error, not observable. Regarding the PS phase, the differences between the two isotherms below the respective P_g values[33] are also not obvious due the relatively

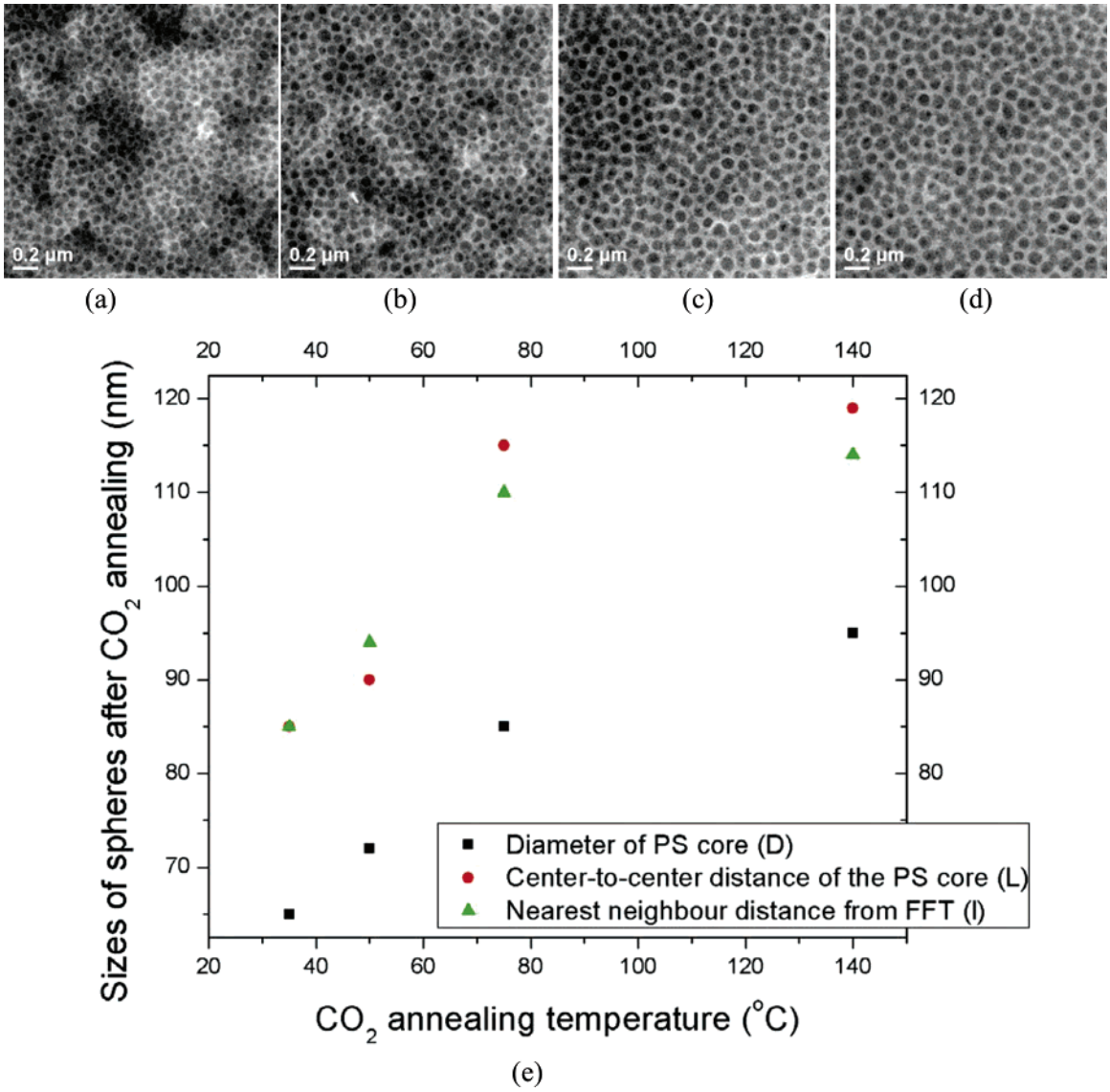

Figure 6. HAADF−STEM images of PS-*b*-PFOMA samples ($h \sim 150-200$ nm) after annealing under various Sc-CO_2 conditions. The annealing conditions are as the following: (a) 35 °C, 6 days; (b) 50 °C, 3 days; (c) 75 °C, 3 days; (d) 140 °C, 25 h; the CO_2 pressure was fixed at 13.8 MPa (2000 psig) for all temperatures. (e) The sizes of PS cores measured from (a−d) as increasing CO_2 annealing temperature. Typical error bars for the diameter of PS cores are 11−13 nm and those for the center-to-center distance of the PS cores are 12−15 nm.

large normal axis scale. On the basis of the experimental conditions in Figure 6a−d, both blocks are expected to be rubbery,[33] and the swelling of each block may be estimated from the corresponding CO_2 activities, listed in Table 4. It is evident that the sorption difference between PS and PFOMA in CO_2 decreases with increasing temperature at constant pressure.

Thus far, we have shown that both the size of PS cores and the relative swelling ratio of PS versus PFOMA increase gradually with increasing CO_2 annealing temperature at constant pressure. Next, we will explain these results based on the classical scaling theory for the formation of block copolymer micelles in a selective solvent. It is well-known that the growth of the micelles is driven by the high surface tension between the core block and the solvent. As micelles grow, the corona chains will become highly stretched and the repulsion of the swollen corona chains will increase. An entropy loss will thus arise as an opposing effect against the micelle growth. For starlike micelles, it is the balance of the two dominant contributions to the free energy of a micelle (the elastic energy of corona and the surface energy of the core) that governs the equilibrium micelle size as well as the aggregation number, whereas the elastic energy of the core is often omitted.[61]

Most theoretical models for micellization of block copolymer can be divided into two categories: "mean field"[62] and "scaling"[61] theories.[63,64] We will follow the "scaling" model developed by Zhulina et al.[61] to examine the contribution of each energy term in the total free energy of the micelles, especially the effects of core and corona chain stretching on the micelles sizes. This "scaling" model developed by Zhulina et al.[61] is constructed so that we can redefine part of the contribution to core size dependence into a new term that characterizes the relative stretching between corona and core chains. It is particularly instructive to examine the dependence of core sizes on this new term given the effect of Sc-CO_2 on chain stretching.

We consider a flexible A-*b*-B diblock copolymer with N_A, $N_B \gg 1$ and with respective monomers sizes of a_A and a_B, selectively, dissolved in a good solvent for A. The free energy of a block copolymer A-*b*-B spherical micelle in the solution is

$$F = F_A + F_S + F_B \quad (3)$$

Here, F_B, F_S, and F_A are the free energy per chain of the micellar

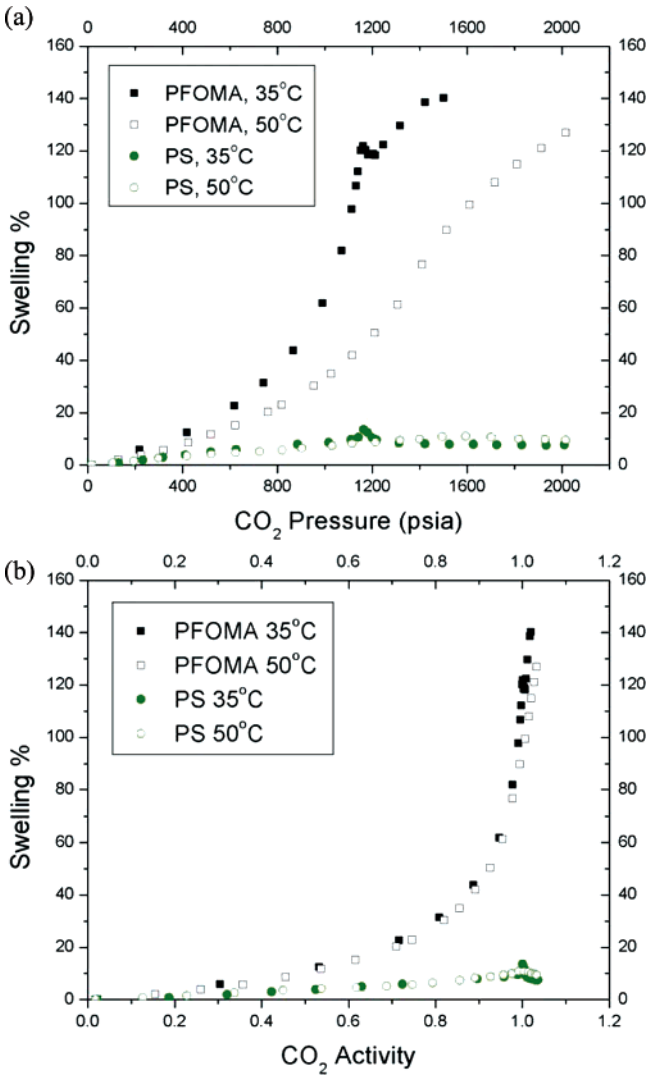

Figure 7. (a) Swelling isotherm for PS and PDHFOMA (for simplicity, indicated by PFOMA on the plot legends) films in Sc-CO_2. (b) Swelling vs CO_2 activity for PS and PDHFOMA films.

core (composed by B), of its surface, and of the corona (composed by A). The elastic free energy per chain for the micellar core due to the stretching of B chains compared with their unperturbed state is[61]

$$F_B = 3\pi^2 r^3/80 p_B N_B \tag{4}$$

Here, $r = R/a_B$ is the dimensionless radius of the core, R is the radius of the spherical core, and p_B is the ratio between the Kuhn segment l_B and the monomer size a_B ($p_B = l_B/a_B$).

The following two assumptions are made: (1) the micellar core composed of B block is partially swollen by the poor solvent; (2) the volume fraction of B block in the micellar core is denoted by Φ, which does not depend on the distance d from its center.[61] Then Φ can be represented by the following equation,[61]

$$\Phi = 3N_B {a_B}^3/(Rs) \tag{5}$$

where s is the surface area per chain. Thus surface free energy per chain is[61]

$$\frac{F_S}{kT} = \tilde{\gamma} s = \gamma(s/{a_B}^2) = \gamma \frac{3N_B a_B}{\varphi R} \tag{6}$$

Here, $\tilde{\gamma}$ is the surface free energy per unit area and $\gamma = \tilde{\gamma} {a_B}^2$ is the surface free energy per area ${a_B}^2$, both divided by kT.

The equilibrium structure of the corona is determined by the balance between the elastic stretching and the repulsive interaction of the A block. Here, the corona of the micelles can be regarded as a melt of correction blobs (region of nonoverlapping chains), which has a thermal energy of kT. Then free energy of the corona may be given by[61]

$$\frac{F_A}{kT} = \upsilon \hat{C}_F r^{3/2} \left(\frac{\Phi}{3N_B}\right)^{1/2} \ln\left[1 + \frac{1}{\upsilon}\left(\frac{a_A}{a_B}\right)^{1/\upsilon} \hat{C}_H N_A r^{(1-3\upsilon)/(2\upsilon)} \left(\frac{3N_B}{\Phi}\right)^{(\upsilon-1)/(2\upsilon)}\right] \tag{7}$$

Here, υ is the scaling exponent and is equal to $^3/_5$ in a good solvent. $\hat{C}_F$ and $\hat{C}_H$ are solvent dependent coefficients. The thickness, H, of the corona is given by[61]

$$H = R\left\{\left[1 + \frac{1}{\upsilon}\left(\frac{a_A}{a_B}\right)^{1/\upsilon} \hat{C}_H N_A r^{(1-3\upsilon)/(2\upsilon)} \left(\frac{3N_B}{\Phi}\right)^{(\upsilon-1)/(2\upsilon)}\right]^{\upsilon} - 1\right\} \tag{8}$$

Combining eqs 7 and 8, one obtains[61]

$$\frac{F_A}{kT} = \hat{C}_F r^{3/2} \left(\frac{\Phi}{3N_B}\right)^{1/2} \ln\left(\frac{H}{R} + 1\right) \tag{9}$$

Hence, the total free energy of block copolymer micelles is

$$\frac{F}{kT} = \frac{3\pi^2 r^2}{80 p_B N_B} + \frac{3N_B \gamma}{\Phi r} + \hat{C}_F r^{3/2} \left(\frac{\Phi}{3N_B}\right)^{1/2} \ln\left(\frac{H}{R} + 1\right) \tag{10}$$

If we assume that $\xi = H/R$, which is the ratio between corona thickness and core radius, then ξ can be related to r by

$$\xi = \left[1 + \frac{1}{\upsilon}\left(\frac{a_A}{a_B}\right)^{1/\upsilon} \hat{C}_H N_A r^{(1-3\upsilon)/(2\upsilon)} \left(\frac{3N_B}{\Phi}\right)^{(\upsilon-1)/(2\upsilon)}\right]^{\upsilon} - 1 \tag{11}$$

ξ is, alternatively, proportional to the ratio between the degree of stretching for the corona and core chains. Recalling that Sw% $= (\Delta V/V_0)$%, we have

$$\xi = \frac{H}{R} = \left(\frac{H/H_0}{R/R_0}\right) \times \frac{H_0}{R_0} = \frac{(V/V_0)_{corona}^{1/3}}{(V/V_0)_{core}^{1/3}} \times \frac{H_0}{R_0} = \left(\frac{Sw\%_{corona} + 100\%}{Sw\%_{core} + 100\%}\right)^{1/3} \times \frac{H_0}{R_0} \tag{12}$$

Here, H_0/R_0 can be calculated from the ratio between PFOMA and PS's end-to-end distance in unperturbed states (Table 1). By minimizing the free energy per chain with respect to the dimensionless radius of the core r (eq 10), we can obtain

$$\frac{\delta F}{\delta r} = \frac{3\pi^2 r}{40 p_B N_B} - \frac{3N_B \gamma}{\Phi r^2} + \frac{3}{2} \hat{C}_F r^{1/2} \left(\frac{\Phi}{3N_B}\right)^{1/2} \ln(\xi + 1) + \hat{C}_F r^{3/2} \left(\frac{\Phi}{3N_B}\right)^{1/2} \frac{1}{(\xi + 1)} \frac{\delta(\xi + 1)}{\delta r} = 0 \tag{13}$$

If we assume that $\xi \gg 1$ ($H \gg R$), then (ref 61 made the same assumption in the Appendix II.1 section)

$$\frac{\delta(\xi + 1)}{\delta r} \sim \frac{(1 - 3\upsilon)}{2} \frac{\xi}{r} \tag{14}$$

Table 4. Swelling % of PS and PFOMA in CO_2 under Four Conditions

T (K)	P (MPa)	CO_2 activity	% swelling (PS)	% swelling (PFOMA)	$K = (Sw\%_{PFOMA} + 100\%)/(Sw\%_{PS} + 100\%)$	$K^{1/3}$
308	13.79	1.036	7.6	138[a]	2.21	1.30
323	13.79	1.032	9.4	127	2.07	1.27
348	13.79	0.957	9.3[a]	63[a]	1.49	1.14
413	13.79	0.701	5.3[a]	21[a]	1.15	1.05

[a] These swelling ratios are based on the estimation from Figure 7b.

For starlike micelles, the stretching free energy F_B of the core block can often be neglected. Thus, eq 13 can be further simplified as

$$\frac{\delta F}{\delta r} = -\frac{3N_B\gamma}{\Phi r^2} + \frac{3}{2}\hat{C}_F r^{1/2}\left(\frac{\Phi}{3N_B}\right)^{1/2} \ln(\xi) + \hat{C}_F r^{1/2}\left(\frac{\Phi}{3N_B}\right)^{1/2}\left(\frac{1-3\upsilon}{2}\right) = 0 \quad (15)$$

Hence

$$r \sim \left(\frac{2\gamma}{\hat{C}_F}\right)^{2/5}\left(\frac{3N_B}{\Phi}\right)^{3/5}\left(\frac{1}{3\ln\xi + (1-3\upsilon)}\right)^{2/5} \sim \left(\frac{\gamma}{\ln\xi}\right)^{2/5}\left(\frac{N_B}{\Phi}\right)^{3/5} \quad (16)$$

Please note here that eq 16 is equivalent to eq AII.2 in ref 61, except that we indicate explicitly how r varies with the relative stretching between corona and core chains by introducing the new term, ξ. The aggregation number (total number of chains per micelle) Q is given by

$$Q = \frac{4\pi r^3\Phi}{3N_B} \sim \left(\frac{\gamma}{\ln(\xi)}\right)^{6/5}\left(\frac{N_B}{\Phi}\right)^{4/5} \quad (17)$$

Equation 16 indicates that the micelle core will grow under one of these three conditions: (1) as the interfacial tension between the core and solvent, γ, increases; (2) as the volume fraction of B block in the swollen core, Φ, decreases, or equivalently as the swelling of core block by the solvent increases; (3) as the relative degree of stretching between corona and core, ξ, decreases. Although the first two conclusions seem quite intuitive, the last one, which shows that the size of micelles is strongly dependent on the relative stretching of corona and core chains, has not been discussed in previous studies.

To compare the above prediction with our experimental results, we first estimated the interfacial tension between PS (27 kg/mole) and CO_2, γ. Different values of γ associated with different molecular weights of PS have been reported,[65,66] and interfacial tension is strongly dependent on molecular weight such that[67]

$$\gamma = \gamma_\infty - \frac{K_e}{M^{2/3}} \quad (18)$$

Here, K_e is a constant and γ_∞ is the interfacial tension at infinite molecular weight. On the basis of eq 18, we estimated the values of γ from two reported PS−CO_2 interfacial tensions, as shown in Table 5. Here the reference values of γ for PS (158 kg/mole) and PS (1.85 kg/mole) at the four CO_2 densities were estimated from Figure 9 in ref 66 and Figure 4 in ref 65, respectively. Consistent with both references, Table 5 shows that the interfacial tension between PS and CO_2, γ, increases with decreasing CO_2 activity. This trend can be understood by considering that the cohesive energy density of CO_2 is much smaller than that of PS. As the CO_2 activity decreases, the difference in cohesive energy densities of CO_2 and PS grows, consequently γ increases.

Table 5. Estimation of the Interfacial Tension between PS (27k) and CO_2

T (K)	P (MPa)	CO_2 density	γ (PS 158k) (dyn/cm)	γ (PS 1.85k) (dyn/cm)	K_e[a]	γ (PS 27k) (dyn/cm)
308	13.79	0.799	8.6	2.5	9.7	7.9
323	13.79	0.666	9.4	3.1	10.1	8.6
348	13.79	0.406	12.1	5.3	10.8	11
413	13.79	0.223	16.6	10.5	9.6	16

[a] Based on $\gamma = \gamma_\infty - K_e/M^{2/3}$, $K_e = (\gamma_1 - \gamma_2)/(M_1^{-2/3} - M_2^{-2/3})$.

Table 6. Effect of CO_2 Annealing Temperature on the Sizes of Micelles Cores

T (K)	P (MPa)	D (nm)	γ (PS 27k) (dyn/cm)	$\xi = K^{1/3} \times (H_0/R_0)$[a]	Φ	$\gamma/(\ln\xi)$ (dyn/cm)
308	13.79	65	7.9	1.79	0.93	14
323	13.79	72	8.6	1.77	0.91	15
348	13.79	85	11	1.57	0.92	24
413	13.79	95	16	1.44	0.95	44

[a] $H_0/R_0 \sim 1.38$, from the ratio between PFOMA and PS's end-to-end distance in unperturbed states.

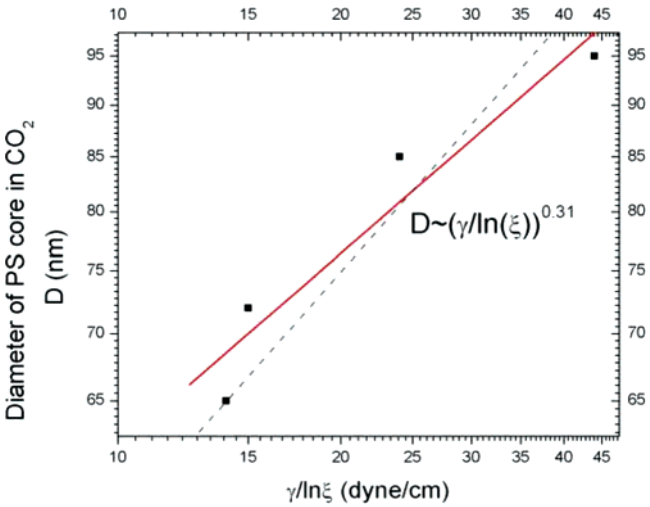

Figure 8. The diameters of PS cores after Sc-CO_2 annealing measured from STEM images vs $\gamma/\ln(\xi)$, where γ is the interfacial tension between PS and CO_2, and $\xi = H/R$ is the relative stretching between corona and core chains. Squares are experimental data, whereas the solid line, with a slope of 0.31, is the linear fit. The broken line has a slope of 0.4, on the basis of eq 16.

Table 6 summarizes the values for ξ, Φ (obtained from Table 4), and γ. Because Φ does not change significantly with CO_2 annealing temperature, its effect on r can be neglected. From Table 6, it is clear that, as the CO_2 annealing temperature increases, or as CO_2 activity decreases, γ increases while the relative stretching between corona and core chains (ξ) decreases. From eq 16, both factors will cause the size of PS cores to increase, consistent with the STEM images. In Figure 8, the measured diameters of the PS core, D, are plotted versus the estimated values of $\gamma/\ln(\xi)$.

The data can be reasonably well described by a power law with an exponent of 0.31. A line with a slope of $^2/_5$, as predicted by eq 16, appears to work equally well, although the following is worth mentioning. First, the scaling model assumes a dilute solution of polymer, whereas the PS-*b*-PFOMA films in CO_2 should be considered as quite concentrated. Second, the size of PS core is large compared with the measured center-to-center distance between the aggregates, partially as a consequence of the ellipsoidal shape. Other scaling models showed that, for micelles with relatively large cores, the dependence of core sizes on γ is weaker.[64] Third, $\xi \gg 1$ is assumed, while the values of ξ obtained from the swelling isotherms are not necessarily much larger than unity (Table 6). Finally, γ is only estimated through reported values for other PS molecular weights, and the swelling of PDHFOMA homopolymer could be different from that of PFOMA block in the diblock. Nevertheless, the key finding is that the scaling model qualitatively predicts that size of PS cores increases with increasing CO_2 annealing temperature, and the observed exponential dependence of D on $\gamma/\ln(\xi)$ agrees, nearly quantitatively, with the model.

It is noteworthy that this trend of increasing micelles size with decreasing CO_2 density is in agreement with related studies on bulk block copolymer micelles dissolved in Sc-CO_2.[68−71] This agreement further suggests that the size dependence of PS-*b*-PFOMA micelles in thin films on CO_2 solvent properties is similar to that of block copolymer micelles dissolved in Sc-CO_2.

4. Conclusions

PS-*b*-PFOMA cast from a cosolvent mixture of toluene and Freon 113 formed a micellar structure, with a PFOMA core and PS corona, on SiO_x/Si substrates. The free surface and polymer/substrate layers were enriched with PFOMA. Upon annealing in Sc-CO_2, the structure underwent an inversion, wherein the PS chain segments formed the core and the PFOMA segments formed the corona. This inversion is associated with the strong affinity of PFOMA with Sc-CO_2. In addition, the sizes of the PS cores were found to increase with decreasing CO_2 activity. A "scaling" model showed that the increasing interfacial tension between PS and CO_2, as well as the decreasing relative stretching between the corona and core chains, led to the increasing aggregates sizes with decreasing Sc-CO_2 activity. The ability to tune the morphology of self-assembled copolymer films with Sc-CO_2 is of practical interest for templating inorganic nanocrystals in block copolymer scaffolds. In a companion study,[59] Au nanocrystals with low-PS oligomers as ligands premixed with the copolymer in solution were found to sequester within the PS domains of PS-*b*-PFOMA films and to follow the structural inversion when annealed in Sc-CO_2. The unique electronic, photonic, magnetic, and mechanical properties of such inorganic nanoparticles can add functionalities to the copolymer/nanoparticle composites, which are very desirable in applications such as the synthesis of photonic crystals and the fabrication of flash memory devices.

Acknowledgment. This work was supported by the STC Program of the National Science Foundation under agreement CHE-9876674, by DMR-0601890, and by the Department of Energy (DE-FG02-04ER15549). We would like to thank Dr. Stephen E. Webber for useful discussions and Dr. Yangming Sun for the help with XPS. We also want to acknowledge the Center for Nano- and Molecular Science and Technology at UT−Austin for STEM and SFM instruments as well as the Welch Foundation and SPRING for partial financial support of these instruments.

References and Notes

(1) Segalman, R. A. *Mater. Sci. Eng. R* **2005**, *48*, 191.
(2) Volkmuth, W. D.; Austin, R. H. *Nature* **1992**, *358*, 600.
(3) Park, M.; Harrison, C.; Chaikin, P. M.; Register, R. A.; Adamson, D. H. *Science* **1997**, *276*, 1401.
(4) Fink, Y.; Winn, J. N.; Fan, S.; Michel, J.; Joannopoulos, J. D.; Thomas, E. L. *Science* **1998**, *282*, 1679.
(5) Chou, S. Y.; Wei, M. S.; Krauss, P. R.; Fischer, P. B. *J. Appl. Phys.* **1994**, *76*, 6673.
(6) Thurn-Albrecht, T.; Schotter, J.; Kastle, G. A.; Emley, N.; Shibauchi, T.; Krusin-Elbaum, L.; Guarini, K.; Black, C. T.; Tuominen, M. T.; Russell, T. P. *Science* **2000**, *290*, 2126.
(7) Pai, R. A.; Humayun, R.; Schulberg, M. T.; Sengupta, A.; Sun, J. N.; Watkins, J. J. *Science* **2004**, *303*, 507.
(8) Zhu, L.; Cheng, S. Z. D.; Calhoun, B. H.; Ge, Q.; Quirk, R. P.; Thomas, E. L.; Hsiao, B. S.; Yeh, F.; Lotz, B. *Polymer* **2001**, *42*, 5829.
(9) Kim, D. H.; Jia, X.; Lin, Z.; Guarini, K. W.; Russell, T. P. *Adv. Mater.* **2004**, *16*, 702.
(10) Kim, D. H.; Kim, S. H.; Lavery, K.; Russell, T. P. *Nano Lett.* **2004**, *4*, 1841.
(11) Sundrani, D.; Darling, S. B.; Sibener, S. J. *Langmuir* **2004**, *20*, 5091.
(12) Morkved, T. L.; Lu, M.; Urbas, A. M.; Ehrichs, E. E.; Jaeger, H. M.; Mansky, P.; Russell, T. P. *Science* **1996**, *273*, 931.
(13) Segalman, R. A.; Yokoyama, H.; Kramer, E. J. *Adv. Mater.* **2001**, *15*, 1152.
(14) Fasolka, M. J.; Harris, D. J.; Mayes, A. M.; Yoon, M.; Mochrie, S. G. J. *Phys. Rev. Lett.* **1997**, *79*, 3018.
(15) Kim, S. O.; Solak, H. H.; Stoykovich, M. P.; Ferrier, N. J.; dePablo, J. J.; Nealey, P. F. *Nature* **2003**, *424*, 411.
(16) Rockford, L.; Liu, Y.; Mansky, P.; Russell, T. P.; Yoon, M.; Mochrie, S. G. J. *Phys. Rev. Lett.* **1999**, *88*, 2602.
(17) Rockford, L.; Russell, T. P.; Yoon, M.; Mochrie, S. G. J. *Macromolecules* **2001**, 34, 1487.
(18) Albalak, R. J.; Thomas, E. L.; Capel, M. S. *Polymer* **1997**, *38*, 3819.
(19) Villar, M. A.; Rueda, D. R.; Ania, F.; Thomas, E. L. *Polymer* **2002**, *43*, 5139.
(20) Bodycomb, J.; Funaki, Y.; Kimishima, K.; Hashimoto, T. *Macromolecules* **1999**, *32*, 2075.
(21) DeSimone, J. M. *Science* **2002**, *297*, 799.
(22) Kazarian, S. G. *Polym. Sci., Ser. C* **2000**, *42*, 78.
(23) Zhang, Y.; Gangwani, K. K.; Lemert, R. M. *J. Supercrit. Fluids* **1997**, *11*, 115.
(24) Zhang, Z.; Handa, P. Y. *Macromolecules* **1997**, *30*, 8505.
(25) Liao, X.; Wang, J.; Li, G.; He, J. *J. Polym. Sci., Part B: Polym. Phys.* **2004**, *42*, 280.
(26) Gross, S.; Roberts, G. W.; Kiserow, D.; DeSimone, J. M. *Macromolecules* **2000**, *33*, 40.
(27) Lambert, S. M.; Paulaitis, M. E. *J. Supercrit. Fluids* **1991**, *4*, 15.
(28) Beckman, E.; Porter, R. *J. Polym. Sci., Part B: Polym. Phys.* **1987**, *25*, 1511.
(29) Arceo, A.; Green, P. F. *J. Phys. Chem. B* **2005**, *109*, 6958.
(30) Vogt, B. D.; Brown, G. D.; RamachandraRao, V. S.; Gupta, R. R.; Lavery, K. A.; Francis, T. J.; Russell, T. P.; Watkins, J. J. *Macromolecules* **2003**, *36*, 4029.
(31) Vogt, B. D.; Brown, G. D.; RamachandraRao, V. S.; Watkins, J. J. *Macromolecules* **1999**, *32*, 7907.
(32) Watkins, J. J.; Brown, G. D.; RamachandraRao, V. S.; Pollard, M. A.; Russell, T. P. *Macromolecules* **1999**, *32*, 7737.
(33) Pham, J. Q.; Johnston, K. P.; Green, P. F. *J. Phys. Chem. B* **2004**, *108*, 3457.
(34) Meli, L.; Pham, J. Q.; Johnston, K. P.; Green, P. F. *Phys. Rev. E* **2004**, *69*, 051601.
(35) Pham, J. Q.; Sirard, S. M.; Johnston, K. P.; Green, P. F. *Phys. Rev. Lett.* **2003**, *91*, 175503.
(36) Sirard, S. M.; Ziegler, K. J.; Sanchez, I. C.; Green, P. F.; Johnston, K. P. *Macromolecules* **2002**, *35*, 1928.
(37) Sirard, S. M.; Green, P. F.; Johnston, K. P. *J. Phys. Chem. B* **2001**, *105*, 766.
(38) Arnold, M. E.; Nagai, K.; Freeman, B. D.; Spontak, R. J.; Betts, D. E.; DeSimone, J. M.; Pinnau, I. *Macromolecules* **2001**, *34*, 5611.
(39) Zhang, L.; Eisenberg, A. *J. Am. Chem. Soc.* **1996**, *118*, 3168.
(40) Arnold, M. E.; Nagai, K.; Spontak, R. J.; Freeman, B. D.; Leroux, D.; Betts, D. E.; DeSimone, J. M.; DiGiano, F. A.; Stebbins, C. K.; Linton, R. W. *Macromolecules* **2002**, *35*, 3697.
(41) Sirard, S. M.; Castellanos, H. J.; Hwang, H. S.; Lim, K. T.; Johnston, K. P. *Ing. Eng. Chem. Res.* **2004**, *43*, 525.
(42) Li, Y.; Loo, Y.-L.; Register, R. A.; Green, P. F. *Macromolecules* **2005**, *38*, 7745.
(43) Turner, M. S.; Rubinstein, M.; Marques, C. M. *Macromelecules* **1994**, *27*, 4986.
(44) Webber, S. E. *J. Phys. Chem. B* **1998**, *102*, 2618.

(45) Webber, G. B.; Wanless, E. J.; Butun, V.; Armes, S. P.; Biggs, S. *Nano Lett.* **2002**, *2*, 1307.
(46) Webber, G. B.; Wanless, E. J.; Armes, S. P.; Baines, F. L.; Biggs, S. *Langmuir* **2001**, *17*, 5551.
(47) Spatz, J. P.; Sheiko, S.; Moller, M. *Macromolecules* **1996**, *29*, 3220.
(48) Regenbrecht, M.; Akari, S.; Forster, S.; Mohwald, H. *J. Phys. Chem. B* **1999**, *103*, 6669.
(49) Meiners, J. C.; Quintel-Ritzi, A.; Mlynek, J.; Elbs, H.; Krausch, G. *Macromolecules* **1997**, *30*, 4945.
(50) Ligoure, C. *Macromolecules* **1991**, *24*, 2968.
(51) Li, Z.; Zhao, W.; Liu, Y.; Rafailovich, M. H.; Sokolov, J.; Khougaz, K.; Eisenberg, A.; Lennx, R. B.; Krausch, G. *J. Am. Chem. Soc.* **1996**, *118*, 10892.
(52) Connell, S. D.; Collins, S.; Fundin, J.; Yang, Z.; Hamley, I. W. *Langmuir* **2003**, *19*, 10449.
(53) Breulmann, M.; Forster, S.; Antonietti, M. *Macromol. Chem. Phys.* **2000**, *201*, 204.
(54) Kim, S. H.; Misner, M. J.; Russell, T. P. *Adv. Mater.* **2004**, *16*, 2119.
(55) Lin, Z.; Kim, D. H.; Wu, X.; Boosahda, L.; Stone, D.; LaRose, L.; Russell, T. P. *Adv. Mater.* **2002**, *19*, 1373.
(56) O'Neill, M. L.; Cao, Q.; Fang, M.; Johnston, K. P.; Wilkinson, S. P.; Smith, C. D.; Kerschner, J. L.; Jureller, S. H. *Ind. Eng. Chem. Res.* **1998**, 37, 3067.
(57) RamachandraRao, V. S.; Gupta, R. R.; Russell, T. P.; Watkins, J. J. *Macromolecules* **2001**, *34*, 7923.
(58) Xu, T.; Hawker, C. J.; Russell, T. P. *Macromolecules* **2005**, *38*, 2802.
(59) Meli, L.; Li, Y.; Johnston, K. P.; Green, P. F., in preparation.
(60) Brown, H. R.; Russell, T. R. *Macromolecules* **1996**, *29*, 798.
(61) Zhulina, E. B.; Adam, M.; LaRue, I.; Sheiko, S. S.; Rubinstein, M. *Macromolecules* **2005**, *38*, 5330.
(62) Nagarajan, R.; Ganesh, K. *J. Chem. Phys.* **1989**, *90*, 1989.
(63) Lund, R.; Willner, L.; Stellbrink, J.; Radulescu, A.; Richter, D. *Macromolecules* **2004**, *37*, 9984.
(64) Linse, P., Modelling of the Self-Assembly of Block Copolymer in Selective Solvent. In *Amphiphilic Block Copolymers*; Alexandridis, P., Lindman, B., Eds.; Elsevier: Amsterdam, The Netherlands, 2000.
(65) Harrison, K. L.; da Rocha, S. R. P.; Yates, M. Z.; Johnston, K. P. *Langmuir* **1998**, *14*, 6855.
(66) Jaeger, P. T.; Eggers, R.; Baumgartl, H. *J. Supercrit. Fluids* **2002**, *24*, 203.
(67) Wu, S. *Polymer Interface and Adhesion*; Marcel Dekker: New York, 1982.
(68) Johnston, K. P.; McFann, G.; Lemert, R. M. *Am. Chem. Soc. Symp. Ser.* **1989**, (406), 140.
(69) Fulton, J. L.; Pfund, D. M.; McClain, J. B.; Romack, T. J.; Maury, E. E.; Combes, J. R.; Samuski, E. T.; DeSimone, J. M.; Capel, M. *Langmuir* **1995**, *11*, 4241.
(70) McClain, J. B.; Betts, D. E.; Canelas, D. A.; Samulski, E. T.; DeSimone, J. M.; Londono, D.; Cochran, H. D.; Wignall, G. D.; Chillura-Martino, D.; Triolo, R. *Science* **1996**, *274*, 2049.
(71) McClain, J. B.; Londono, D.; Combes, J. R.; Romack, T. J.; Canelas, D. A.; Betts, D. E.; Wignall, G. D.; Samulski, E. T.; DeSimone, J. M. *J. Am. Chem. Soc.* **1996**, *118*, 917.

MA060960R